International Journal for Multidisciplinary Research (IJFMR)
E-ISSN: 2582-2160 ● Website: www.ijfmr.com ● Email: editor@ijfmr.com

Aerodynamic Performance Enhancement of Low Aspect Ratio Military Drone Aircraft Wing Through Employing Leading Edge Tubercles

Syed Abdullah Al Mamun

Wing Commander, Bangladesh Air Force

Abstract

Present study aim to improve the aerodynamic performance of low Aspect Ratio (AR) military drone aircraft wing, through employing leading edge tubercle. For that purpose two wing model were design one with smooth leading edge and second with tubercle leading edge. The wing models were developed by using NACA0012 airfoil profile, whereas tubercles of amplitude 5% of chord (c) and wavelength of 11% of c is employed. The numerical simulation as performed at chord based Reynolds number of 140000 in pre-stall and post stall regime. The computational fluid dynamic simulation is performed at different angle of attack ranging from 0^o to 25^o with the interval of 5^o. Computational Fluid Dynamics (CFD) results reveal that tubercle at the leading edge of the low AR wing has favorable effect on the wing performance. Aerodynamic performance of both smooth leading edge and tubercle leading edge wing is similar up to 15^o angle of attack, whereas at 20^o and 25^o significant improvement in Lift-to-Drag L/D ratio is observed. It is estimated that at maximum increment of 53% in lift coefficient ii achieved at 25^o angle of attack for as compared to smooth LE wing model. Moreover, maximum 20.5% decrease in drag coefficient is estimated in case of tubercle leading edge as compared to baseline model at 20^o angle of attack. The critical observation of field around the tubercle leading edge wing is found that tubercles restrict flow separation through generation of low strength vortices; these vortices enhance momentum exchange within the boundary layer.

Keywords: Aerodynamics, CFD, Low Aspect Ratio, Leading Edge Tubercles, Drone

1. Introduction

Improving the aerodynamic performance of airfoil/ wing has remained the interest of aerodynamics researchers. Over the years of research numerous flow control techniques have been developed to improve the aerodynamic performance of civil and military aircrafts. Those flow control techniques has been divided into two groups active flow control and passive flow control. Active flow control system requires extra energy to operate and major active flow control techniques are flaps, slots, boundary layer suction and blowing and so on. Whereas passive flow control is simple, easy to implement, requires no extra energy and the widely employed passive control techniques are winglet, vortex generator, gurney flap and leading edge tubercles. The concept of tubercles at the leading edge of the wing received attention after the work Fish and Battle [1, 2], the idea of employing tubercles at the leading edge of the wing has emerged during the morphological study of the Humpback whale, study found that despite of large size Humpback whale is capable of performing sharp turns during its prey. It is only possible if

humpback maintain its lift coefficient at higher angle of attack without significant stall. The detailed analysis of Humpback flippers revealed that round protuberance shapes at its flipper is unique than other aerobatic animals. Moreover, over the last few years numerous studies has been carried out to control flow in the subsonic [3-13] and the transonic flow regimes [14-17]. The deployment of tubercle in various rotating fluid machinery application such as propeller [18, 19], wind turbines [18, 20-30] and on the tidal turbine[31-33] to improve their aerodynamic performance, by controlling dynamic stall is gaining research attention over last decade.

In addition to this, flow separation is the major problem, which degrades aircraft wing aerodynamic performance at higher angle of attack. Moreover, the special requirement such as short-take-off and landing, in this situation aircraft requires to cruise at high angle of attack, as results of which flow separation occurs causing to reduce lift and increase drag. Furthermore, in case of small size Unmanned Arial Vehicles (UAVs), these vehicles operates at low Reynolds number, where flow separation occurs even at low angle of attacks, thus in order to improve the aerodynamic performance of low aspect ratio military drone aircraft wing is need to conducted in detail. Moreover, the numerous studies have been conducted to analyze the aerodynamic performance of the aircraft wing.

Recently a numerical study is conducted [34] to investigated the effect of changing wavelength of a finite wingspan and studied the flow behavior in pre-stall and post-stall regimes. Two different wavy models are used named as (λ0305h1) and (λ0503h1) with increasing wavelength and decreasing wavelength from root to tip respectively. Both wing models were simulated at chord based Reynolds number of 1.2×10^5. Numerical simulation results revealed that the L/D ratio decreases in pre-stall regime. It is estimated that 16.89% and 4.22% for (λ0503h1) and (λ0305h1) wavy wing model respectively. It was also observed that the waviness of wing is only beneficial for post-stall regime. Another study [35] analyzed the aerodynamic performance of the NACA634-021 airfoil wings with different tubercles setups and performed the analysis on finite and infinite wing situations. Study results found that high amplitude leads to gentler stall and moderate wavelength increase the lift. The oil flow visualization was employed to analyze the flow behaviour over the wing models. The LSBs are formed on wavy wing model at lower pitch points are exposed by the pleasant fluorescent images. Another study [36] has accrued out direct numerical simulation to analyze the aerodynamic performance of the NACA0012 airfoil at Reynolds number of 1000. The direct numerical simulations were conducted by using the Spectral/hp Element method to observe the waviness impact on airfoil aerodynamic performance. Numerous combinations of amplitudes and wavelength were implemented to analyze waviness parameters impact on airfoil aerodynamics. Simulation results revealed that waviness results decrease in airfoil aerodynamic performance.

The extensive literature review reveal that most of studies either implemented tubercles on the airfoil and some studies analyzed impact of tubercles at very low Reynolds number not suitable for military drone applications application. In this regards, present study employed tubercles at low aspect ratio rectangular aircraft wing and analyzed its aerodynamic performance at Reynolds number suitable for military drone applications.

2. Numerical modeling

2.1 CAD modeling and meshing

To analyze the impact of employing leading edge tubercles on the military drone aircraft wing, two wing models were developed one with smooth leading edge (i.e baseline model) and second one with tubercle

leading Edge (i.e TLE). The NACA0012 airfoil is selected, and airfoil coordinates were obtained from university of Urbana illunus website. Moreover, both wing models were developed with aspect ratio of (*AR=1*). Both wing models were developed in Pro-Engineer software, further initially 2D airfoil is generated with the coordinates. The 3D CAD model is then developed with the chord length of *c=140 mm*, whereas tubercle at the leading edges were employed through changing the chord length of the airfoil and through employing coordinate transformation equation (1) written as follow.

$$\bar{X} = c + \xi(Z) = c - \frac{h}{2}\cos\left(\frac{2\pi}{\lambda} z\right) \quad (1)$$

In the above Eq. (1) $\bar{X}$ denotes the transformation at specific spanwise location, chord length is denoted with *c* and *Z* is the length in spanwise direction. Moreover, the tubercles amplitude and wavelength are denoted with *h* and λ respectively. The designed three dimensional (3D) CAD model of the smooth and tubercle leading edge wing is presented in Fig. 1(a & b). Furthermore, the tubercle employed on the leading edge of the military drone aircraft wing have wavelength 11% of *c* and the amplitude 5% of chord (*c*).

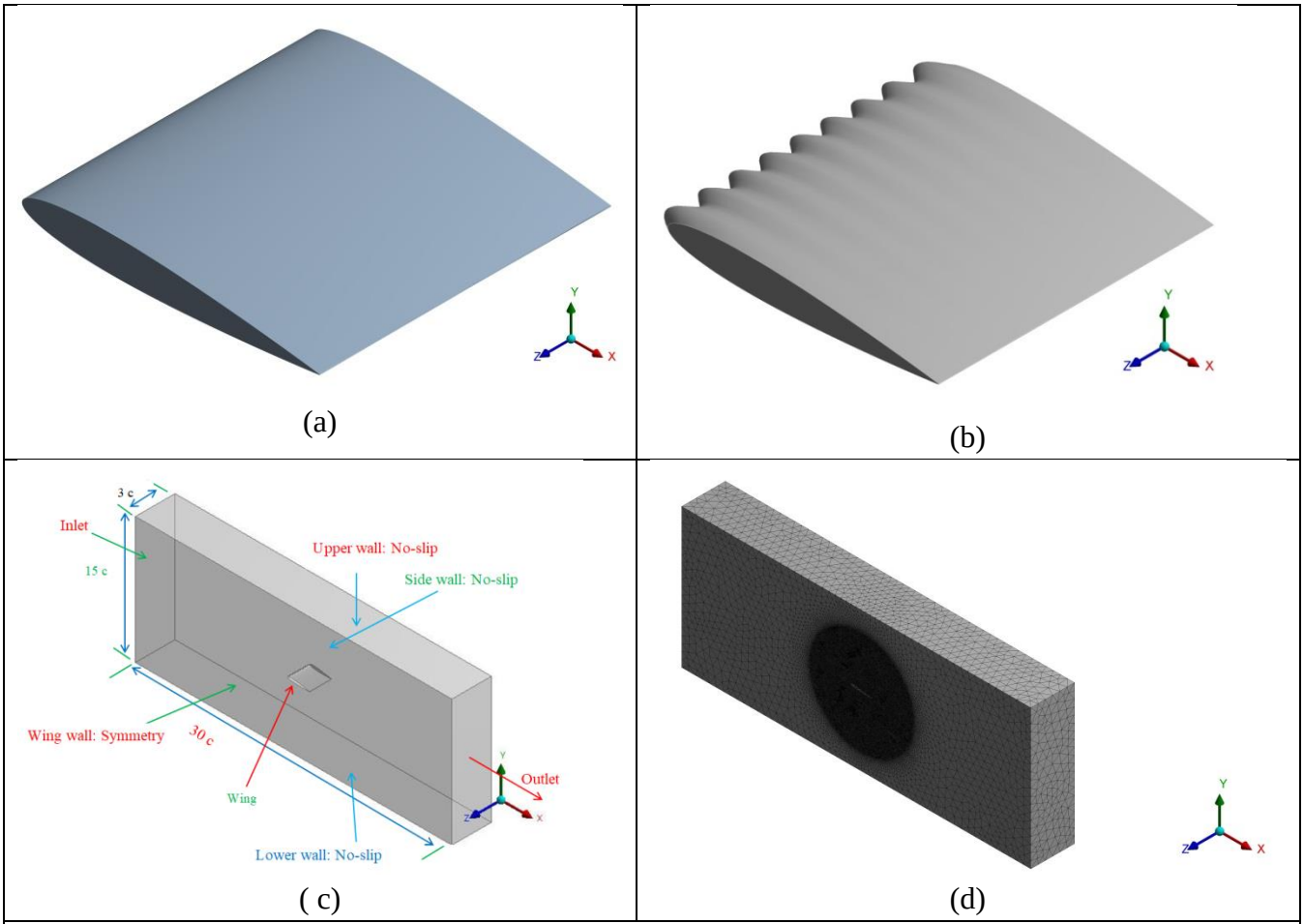

Fig. 01 The designed CAD model (a) the isometric view of the smooth leading edge wing (i.e baseline wing model), (b) the isometric view of tubercle leading edge wing (i.e TLE wing), (c) computational domain created around the wing to generate flow field (d) the meshed model of the computational domain with fine mesh elements near wing

Once the 3D CAD model of the baseline and tubercle leading edge wing model is developed then, the CAD model is imported to the ANSYS Design modeler for further processing. After importing wing model, it is pitched at the desired angle of incidences as in present study wing model is pitched to six different angle of attacks. Once is wing model is pitched to desired angle then fluid domain is created around the solid wing model. The fluid domain size is defined in terms of chord length of wing, fluid domain is extended 10c in upstream and 10c in the downstream direction. Whereas 5c in lateral directions above and below wing surface. Furthermore, 3 times the chord is extended in spanwise direction. To predict aerodynamic performance and 3D flow effects more accurately, one end of the wing is fixed with the symmetry wall as it is attached with the fuselage and the tip of the wing is free. The fluid domain generated around the wing model is discussed and presented in Fig. 01 (c). Once the fluid domain is created then the wing model is further processes in ANSYS meshing tool, where different face were named accordingly and the continuous fluid domain is discretized. Tetrahedral mesh elements used employed to discretize the continuous fluid domain; moreover the unstructured meshing is performed to reduce computational resources and computational time. The elements of 5mm were used to discretized whole computational except the region near the solid. In the closer vicinity of the solid wing sphere influence is created with diameter of 4 times the chord to refine mesh near the solid body. The element size inside the sphere influence is kept 1.5mm for accurate prediction boundary layer impact. Mesh is developed with total number of 2.6×10^7 of cells were generated. The meshed model of the computational domain is presented in Fig. 01(d).

2.2 CFD modeling

Once the meshing is completed, then discretized computational domain is transferred to FLUENT™ for further processing. CFD modeling requires the assumption, boundary condition and operating condition, since the Reynolds number used in present study is low and Mach number is below 0.3 thus assumption of incompressibility remain valid. Thus pressure-based solver is employed, steady state flow simulation is performed up to 15^o angle of attack and unsteady simulation is performed at 20^o and 25^o angle of attack. Air is used as working fluid and no-slip condition is applied on the surface and other three faces of the computational domain presented in Fig. 01(c). In addition to this, symmetry condition is applied on the wall that is attached to military drone aircraft wing. Two turbulence models were selected to encounter the effect of fluctuating component present with the flow field. Finite Volume Method (FVM) is employed to solve the governing fluid flow equations. The uniform velocity operating condition is employed at the inlet with the turbulence intensity of 0.8% is applied, the direction cosine for the velocity is (1, 0, 0). Outlet is defined through pressure outlet and pressure at outlet is set as zero. Furthermore, the governing fluid flow equation were solved through employing SIMPLE scheme and spatial discretization is carried out through second order upwind scheme.

2.3 Computational Model

The present study is conducted at low Reynolds number thus flow is considered as incompressible thus pressure based solver is employed. Moreover flow is considered as viscous, steady at low angle of attack and unsteady at 15^o and 20^o angle of attack. Air is used as working fluid that flows over the wing surface. Thus the governing fluid flow equations, such and continuity equation and momentum equation after employing Reynolds decomposition also known as Reynolds Average Navier stokes (RANS) equations for steady viscous and incompressible flow can be written as follow.

$$\frac{\partial U_i}{\partial x_i} = 0$$

$$\frac{\partial}{\partial x_j}\left(\rho U_i U_j\right) = -\frac{\partial P}{\partial x_i} + \frac{\partial}{\partial x_j}\left[\mu\left(\frac{\partial U_i}{\partial x_j} + \frac{\partial U_j}{\partial x_i}\right)\right] + \frac{\partial}{\partial x_j}\left(-\rho\overline{u_i'}\overline{u_j'}\right)$$

The values of $i,j=1,2,3$ (2)

The last term in above equation (2) is produced as result of Reynolds decomposition and is known as Reynolds stresses ($-\rho\overline{u_i'}\overline{u_j'}$), this term take into account the effect of fluctuations present with the flow. In Fluent [TM] numerous turbulence models are available to accurately model these fluctuations; however each model has merits and demerits. Moreover, the all developed turbulence models are mostly suitable for specific flow conditions. Present employed realizable $k-\varepsilon$ and $k-\omega$ Shear Stress Transport (SST) model. The $k-\varepsilon$ realizable turbulence model is used at low angle of attacks up to 10^o, since numerous studies employed it to analyze the aerodynamic performance of TLE wing [25, 37-40], whereas $k-\omega$ SST turbulence model is employed at high angle attacks such as 15^o and 20^o since the numerous studies suggested that $k-\omega$ SST turbulence model is suitable of near wall and separated flows[25, 40-42], the equation of realizable $k-\varepsilon$ model is written in flowing manner.

$$\frac{\partial\left(ku_j\right)}{\partial x_j} = \frac{\partial}{\partial x_j}\left[\left(\nu + \frac{\nu_t}{\sigma_k}\right)\frac{\partial k}{\partial x_j}\right] + P - \varepsilon$$

And

$$\frac{\partial\left(\varepsilon u_j\right)}{\partial x_j} = \frac{\partial}{\partial x_j}\left[\left(\nu + \frac{\nu_t}{\sigma_\varepsilon}\right)\frac{\partial \varepsilon}{\partial x_j}\right] + C_1 S\varepsilon - C_2\frac{\varepsilon^2}{k+\sqrt{\nu\varepsilon}}$$

Where

$$C_1 = \max\left[0.43, \frac{\eta}{\eta+5}\right]$$

$$\eta = S\frac{k}{\varepsilon}$$

$$S = \sqrt{2S_{ij}S_{ij}}$$

In the above equations, σ_k and σ_ε are turbulent Prandtl numbers for σ_k and σ_ε are k and ε, respectively, whereas generation of turbulence kinetic energy because of the mean velocity gradients is denoted by P. The present study employed model constants as $C_2 = 1.9$, $\sigma_k = 1$, and $\sigma_\varepsilon = 1.2$.

$$\frac{\partial\left(ku_i\right)}{\partial x_j} = \frac{\partial}{\partial x_j}\left(\frac{\Gamma_k \partial k}{\rho \partial x_j}\right) + P + Y_k$$

$$\frac{\partial\left(\omega u_i\right)}{\partial x_j} = \frac{\partial}{\partial x_j}\left(\frac{\Gamma_\omega}{\rho}\frac{\partial \omega}{\partial x_j}\right) + G_\omega - Y_\omega + D_\omega$$

In these equations, P represents the generation of turbulent kinetic energy due to mean velocity gradients and G_ω represents the generation of ω. Γ_k and $\Gamma_\omega \omega$ represents the effective diffusivity of k and ω, respectively. Y_k and Y_ω represent the dissipation of k and ω, respectively, due to turbulence. D_ω represents the cross-diffusion term.

3. Results and Discussion

3.1 Aerodynamic Forces

The aerodynamic forces acting on the baseline and tubercle leading edge wing is discussed and presented in Fig. 2 & 3 in pre-stall and in post-stall regime. The aerodynamics force like lift and drag are produced as a result of pressure stress distribution and shear stress variation. The lift force is produced as a result of pressure difference between the upper and lower surface of the wing. Once the CFD simulation is conducted numerical values of lift and drag forces can be found and lift coefficient (C_L) and coefficient of drag (C_D) is determined from by using following relationship.

$$C_L = \frac{F_L}{1/2\rho U_\infty^2 cL}$$

$$C_D = \frac{F_D}{1/2\rho U_\infty^2 cL} \qquad (9)$$

Whereas in above equations F_L denotes the lift force and F_D represent the drag force, ρ, U_∞ and L denotes density of the air, freestream velocity and span length respectively.

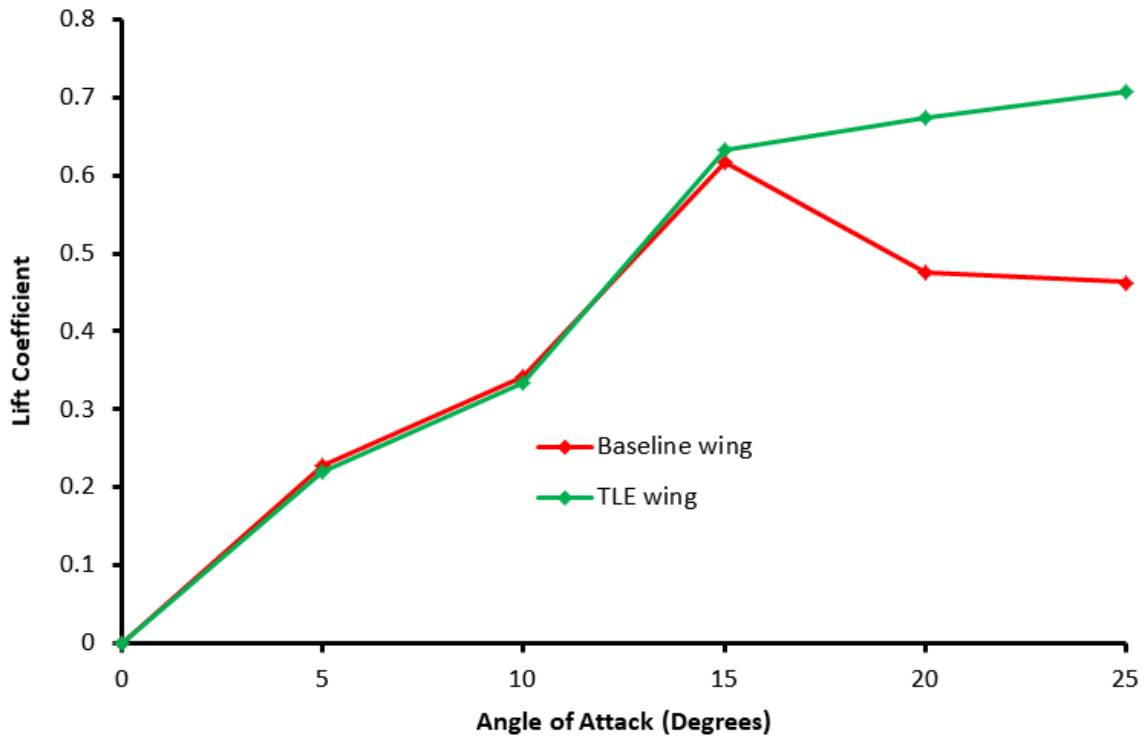

Fig. 2 The variation of lift coefficient for smooth leading edge and tubercle leading edge wing against angle of attack

The lift coefficient over the baseline and TLE wing against angle of attack is plotted in Fig. 2, it is observed from the graph that baseline wing have slightly high lift coefficient up to 10^o angle of attack,

whereas from at 15° AoA TLE wing lift coefficient is higher than the smooth LE wing and difference at higher angles increase further. After 15° angle of attack smooth LE wing under goes stall and lift coefficient fall suddenly, in contrast lift coefficient of TLE wing remain increasing with angle of attack. The drag coefficient variation is for baseline and tubercle leading edge wing is plotted against the angle of attacks is discussed and presented in Fig. 3. It is observed from the drag coefficient both models have similar drag coefficient behavior up to 15° angle of attack. However, at higher angle of attacks such as 20° and 25° the drag coefficient of baseline wing model is significantly higher than tubercle leading edge wing model.

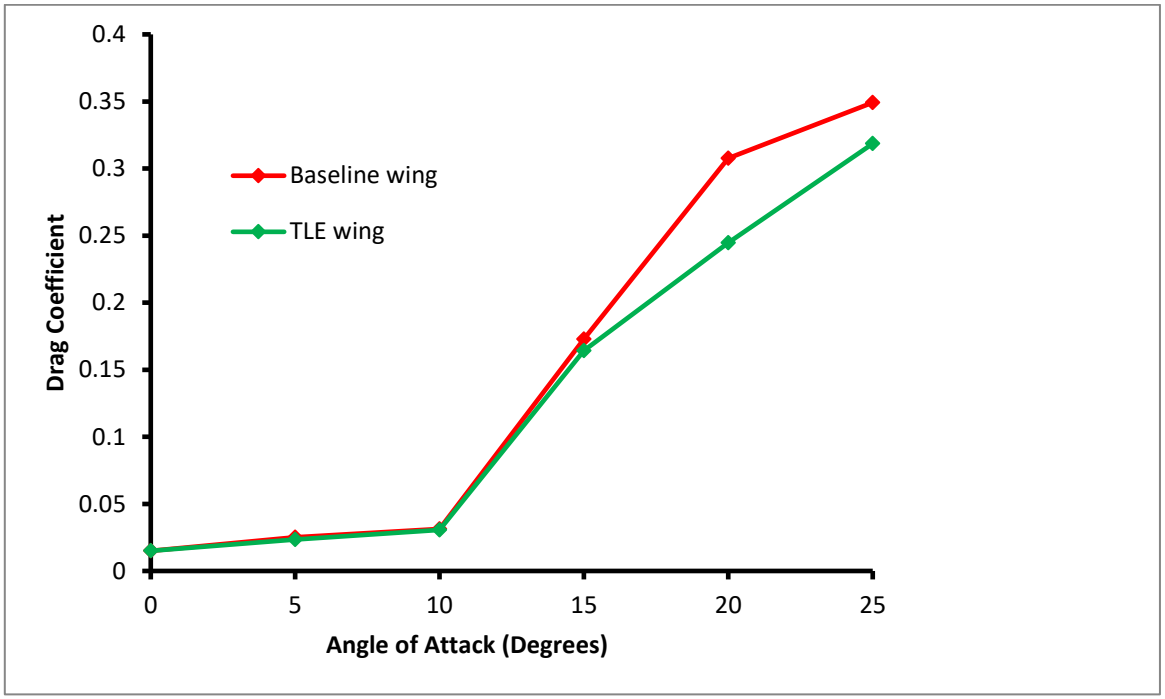

Fig. 3 The variation of drag coefficient for smooth leading edge and tubercle leading edge wing against angle of attack

The variation of the Lift-to-Drag (L/D) ratio is plotted against selected angle of attacks, discussed and presented in Fig. 4. From the L/D ratio of smooth LE and tubercle leading edge wing it is observed that both wing models have similar L/D ratio up to 15° angle of attack. Moreover, from the graph it is also noticed that both wing models experience stall between 10° and 15° angle of attack. From the L/D ratio graph it is observed that tubercle leading edge wing model have significantly higher L/D ratio as compared to smooth leading edge wing model in post-stall regime. This showed that deployment of tubercles at the leading edge of low aspect ratio wing have shown favorable impact on the wing aerodynamic performance in both pre-stall and post-stall regimes.

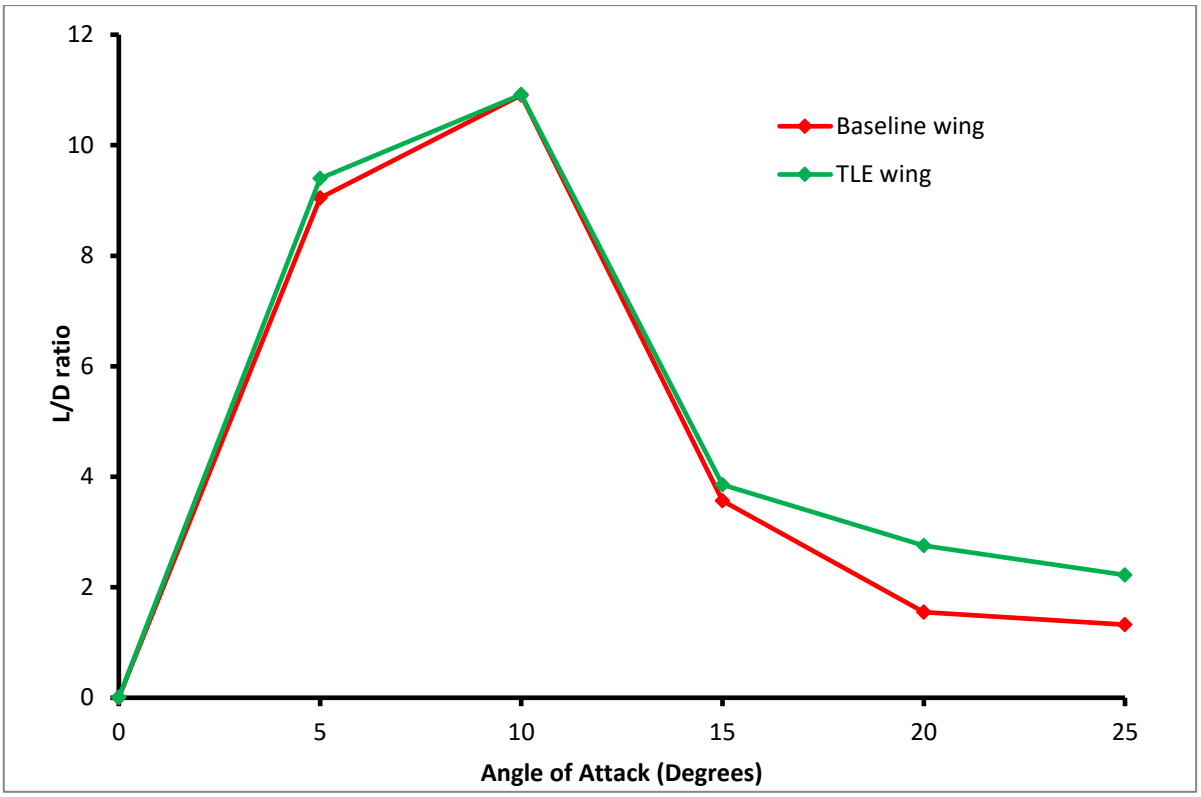

Fig. 4 The variation of L/D ratio against angle of attack for smooth leading edge and tubercle leading edge wing.

3.2 Surface pressure distribution

The static pressure distribution over the baseline and tubercle leading edge wing model is discussed and presented in Fig. 5 (a & b). The static pressure distribution is presented at 5^{o} angle of attack because similar behaviour is observed at other tested angles. From the static pressure distribution over the baseline wing model it is observed that leading edge suction over the complete leading of wing except in small region close to free end of wing. However, in case of the tubercle leading edge wing LE suction is noticed only in the trough region, where at tubercle valley/trough strong leading edge suction enable airfoil to maintain lift coefficient closer to that of the smooth leading edge wing. The comparison of static pressure over both wing models reveal that reduction in leading edge suction in case of TLE wing is compensated with lower magnitude of leading edge suction in case smooth leading edge wing. Moreover, restriction of leading edge suction at tubercle valley causes the spanwise flow in case of tubercle leading edge wing model.

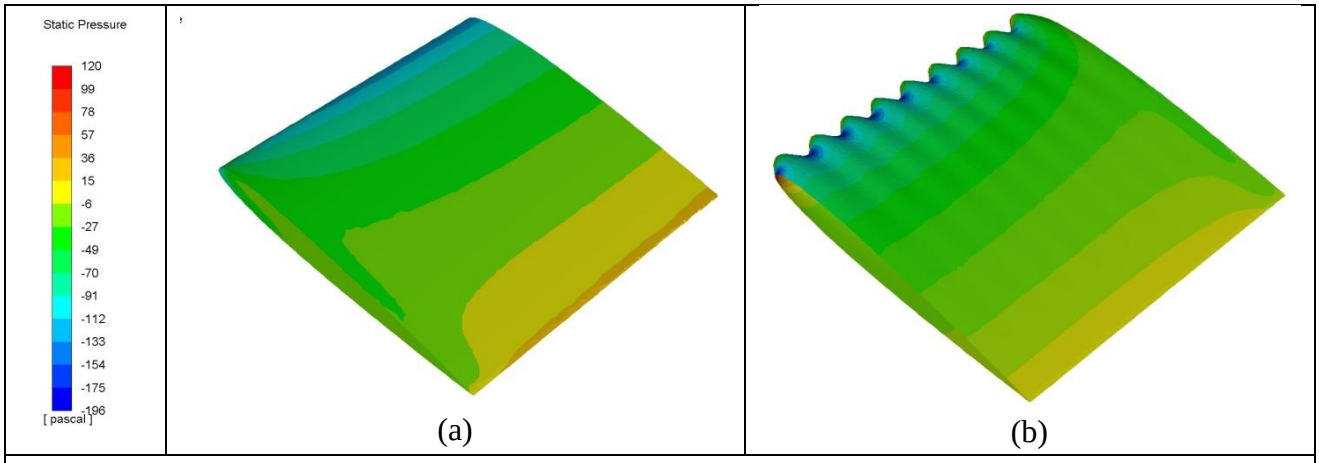

Fig. 5 Static pressure distribution at 5º angle of attack over the (a) smooth leading edge wing (b) Tubercle leading edge wing

In order to clearly understand the aerodynamic behaviour at high angle of attack in post-stall regime, velocity vectors at 25º angle of attack is discussed and presented in Fig. 6(a-c). the velocity vectors over the baseline model is presented in Fig. 6(a), it is observed that flow separation start from leading edge then reattached approximately at 0.35c to 0.4c and then again separated near the trailing edge forming strong flow recirculation zone, as a result pressure difference over the wing upper and lower surface of the wing is decreased resulting in loss of lift coefficient. Moreover, velocity vector distribution over the tubercle leading edge wing valley and peak is presented in Fig. 6(b & c). It is observed from the velocity vector distribution over the TLE wing at tubercle significantly reduced flow separation and tubercles also reduced size recirculation zone.

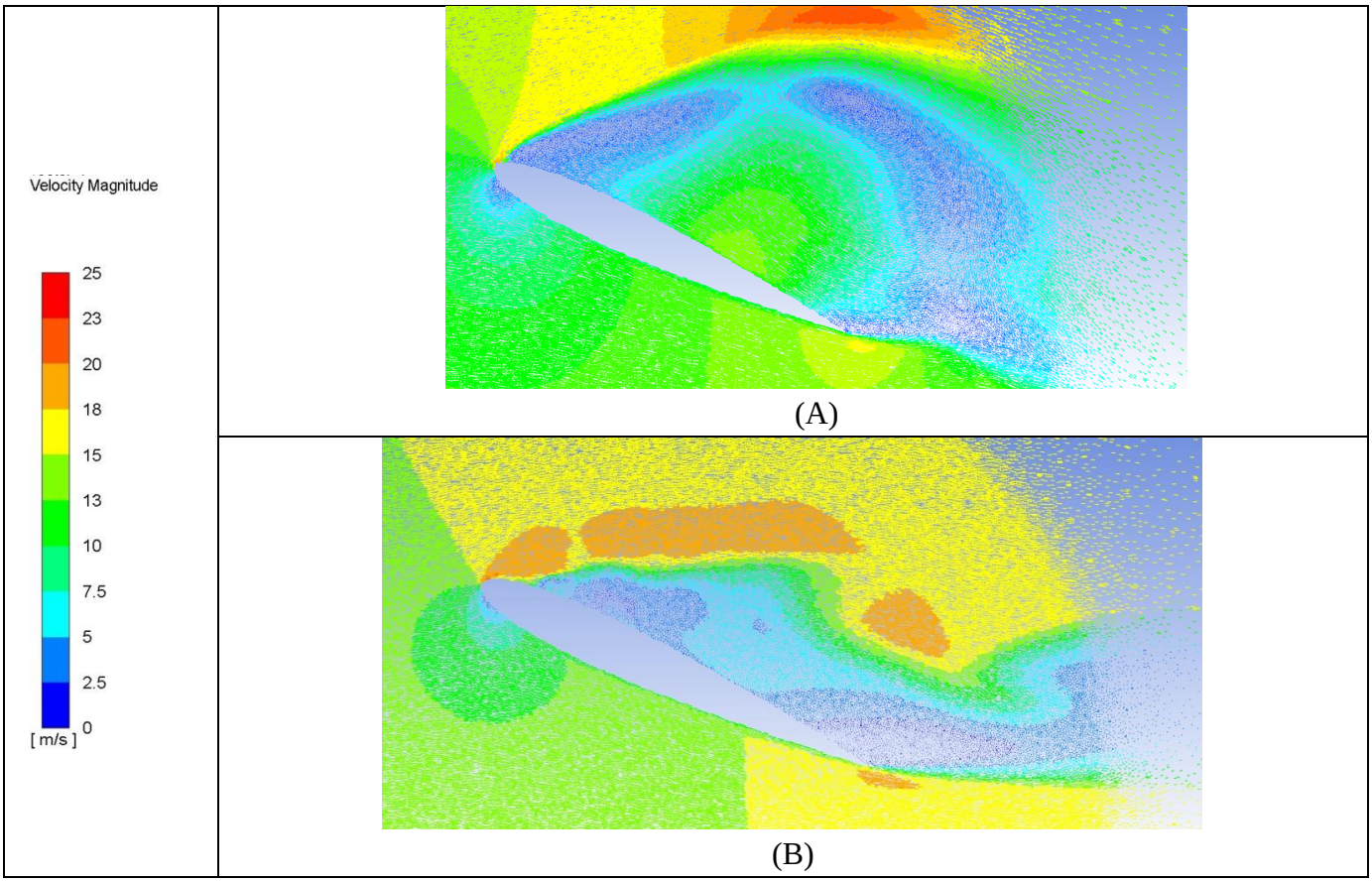

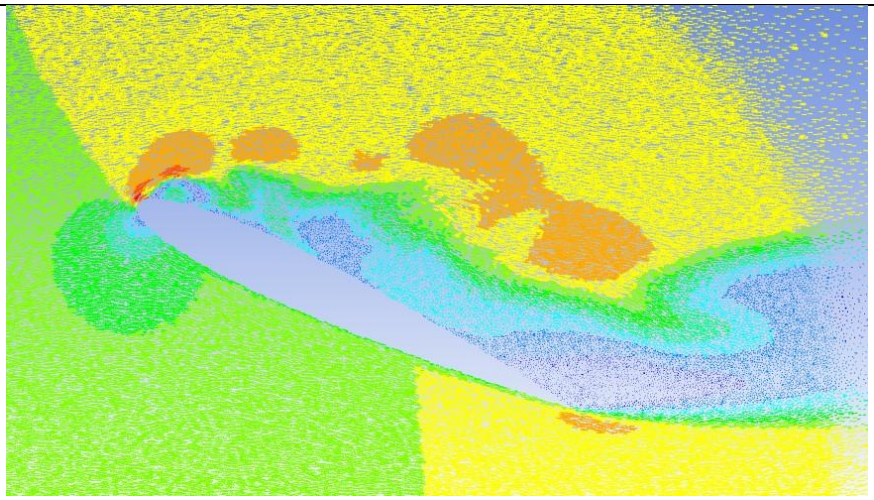

(C)

Fig. 6 Velocity vector distribution at 25º angle of attack over (a) smooth leading edge wing (b) tubercle leading edge wing at valley and (c) tubercle leading edge wing at tubercle peak.

3.3 Flow Mechanism

The streamline flow behaviour the smooth leading and tubercle leading edge wing is discussed and presented in Fig. 7(a-f). Moreover the streamline behavior is discussed and presented at 25^{o} angle of attack. From the streamline behaviour over the baseline wing in Fig 7(a) is observed that strong vortices are produced and create strong flow recirculation zone, similar behaviour is noticed in isometric view of streamline presented in Fig. 7(b). Additionally the streamline flow behaviour over the tubercle leading edge wing peak and valley is discussed and presented in Fig. 7(c-f). From the streamline behaviour it is noticed that vortices produced over TLE wing have low strength and they are not distributed over the wing surface. Moreover, the reduction of vortices strength due to implementation of tubercle help reduced size of flow recirculation zone and also flow separation. The deployment of tubercles creates low strength vortices that enhance momentum exchange within boundary layer and restrict flow separation. Thus, improve the aerodynamic performance in post stall regime.

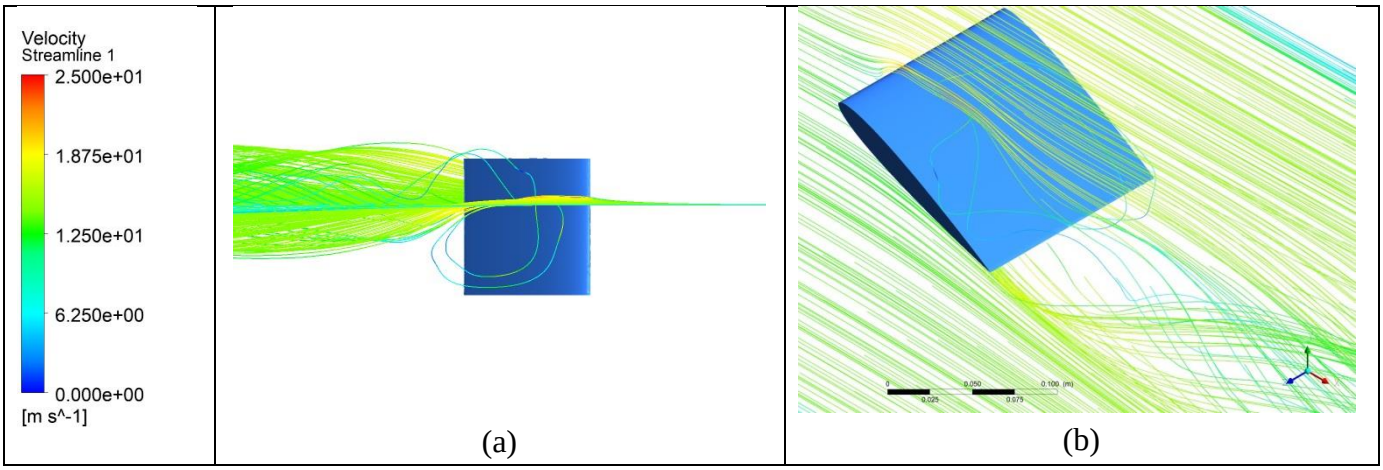

(a) (b)

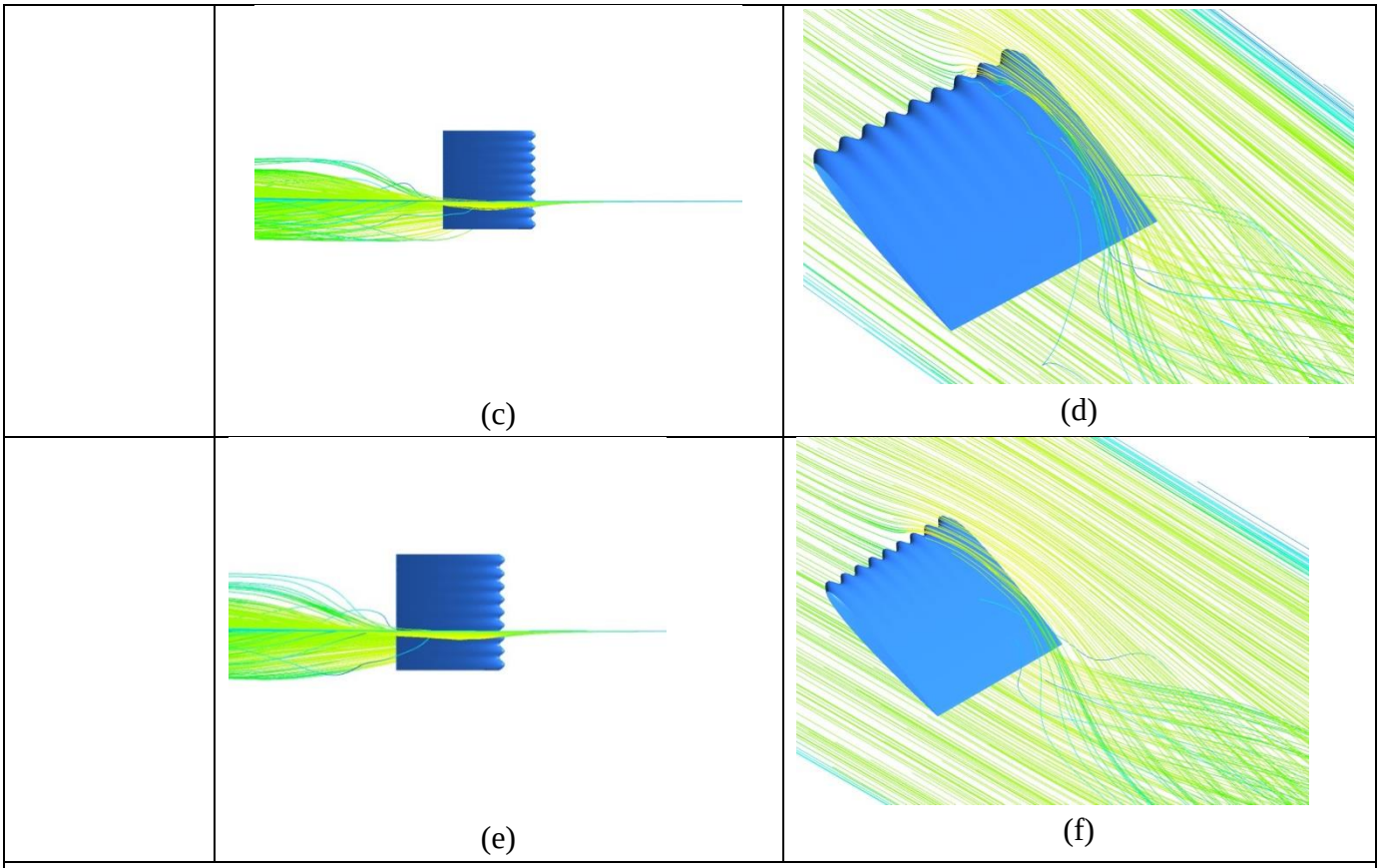

Fig. 7 The streamline flow behaviour at 25º angle of attack over the (a & b) Smooth leading edge wing (c & d) Tubercle Leading edge wing at tubercle peak (e & f) Tubercle Leading edge wing at tubercle valley/ trough

4. Conclusion

This research work analyzed the aerodynamic performance of low aspect ratio military drone aircraft wing by using tubercles at its leading edge. The two wing models smooth leading edge and tubercle leading edge were developed by suing NACA0012 airfoil. The study carried out at chord based Reynolds number of 140000 in pre-stall and post stall regime. The numerical simulation results found that tubercle leading edge wing has shown comparable aerodynamic performance to that of the smooth leading edge wing in pre-stall regime. In addition this TLE wing has higher lift coefficient as compared to the baseline wing model in post-stall regime. Numerical simulation results reveal that tubercle at the leading edge of the low AR wing has favorable effect on the wing performance. Aerodynamic performance of both smooth leading edge and tubercle leading edge wing is similar up to 15^o angle of attack, whereas at 20^o and 25^o significant improvement in Lift-to-Drag L/D ratio is observed. It is estimated that at maximum increment of 53% in lift coefficient ii achieved at 25^o angle of attack for as compared to smooth LE wing model. Moreover, maximum 20.5% decrease in drag coefficient is estimated in case of tubercle leading edge as compared to baseline model at 20^o angle of attack. The critical observation of field around the tubercle leading edge wing is found that tubercles restrict flow separation through generation of low strength vortices; these vortices enhance momentum exchange within the boundary layer.

References

1. F. Fish and G. V. Lauder, "Passive and active flow control by swimming fishes and mammals," *Annu. Rev. Fluid Mech.*, vol. 38, pp. 193-224, 2006.
2. F. E. Fish and J. M. Battle, "Hydrodynamic design of the humpback whale flipper," *Journal of morphology*, vol. 225, pp. 51-60, 1995.
3. C. Cai, S. Liu, Z. Zuo, T. Maeda, Y. Kamada, Q. a. Li, *et al.*, "Experimental and theoretical investigations on the effect of a single leading-edge protuberance on airfoil performance," *Physics of Fluids*, vol. 31, p. 027103, 2019.
4. K. L. Hansen, R. M. Kelso, and B. B. Dally, "Performance variations of leading-edge tubercles for distinct airfoil profiles," *AIAA journal*, vol. 49, pp. 185-194, 2011.
5. K. L. Hansen, N. Rostamzadeh, R. M. Kelso, and B. B. Dally, "Evolution of the streamwise vortices generated between leading edge tubercles," *Journal of Fluid Mechanics*, vol. 788, pp. 730-766, 2016.
6. J. W. Kim, S. Haeri, and P. F. Joseph, "On the reduction of aerofoil–turbulence interaction noise associated with wavy leading edges," *Journal of Fluid Mechanics*, vol. 792, pp. 526-552, 2016.
7. R. Pérez-Torró and J. W. Kim, "A large-eddy simulation on a deep-stalled aerofoil with a wavy leading edge," *Journal of Fluid Mechanics*, vol. 813, pp. 23-52, 2017.
8. N. Rostamzadeh, K. Hansen, R. Kelso, and B. Dally, "The formation mechanism and impact of streamwise vortices on NACA 0021 airfoil's performance with undulating leading edge modification," *Physics of Fluids*, vol. 26, p. 107101, 2014.
9. N. Rostamzadeh, R. Kelso, B. Dally, and K. Hansen, "The effect of undulating leading-edge modifications on NACA 0021 airfoil characteristics," *Physics of fluids*, vol. 25, p. 117101, 2013.
10. S. Sudhakar, N. Karthikeyan, and L. Venkatakrishnan, "Influence of leading edge tubercles on aerodynamic characteristics of a high aspect-ratio UAV," *Aerospace Science and Technology*, vol. 69, pp. 281-289, 2017.
11. H. E. Tanürün and A. Acır, "Investigation of the hydrogen production potential of the H-Darrieus turbines combined with various wind-lens," *International Journal of Hydrogen Energy*, vol. 47, pp. 23118-23138, 2022.
12. Y. Zhang, X. Zhang, L. Yi, M. Chang, and X. Jiakuan, "Aerodynamic performance of a low-Reynolds UAV with leading-edge protuberances inspired by humpback whale flippers," *Chinese Journal of Aeronautics*, vol. 34, pp. 415-424, 2021.
13. Z. Wei, T. H. New, L. Lian, and Y. Zhang, "Leading-edge tubercles delay flow separation for a tapered swept-back wing at very low Reynolds number," *Ocean Engineering*, vol. 181, pp. 173-184, 2019.
14. E. Degregori and J. W. Kim, "An investigation on a supercritical aerofoil with a wavy leading edge in a transonic flow," *Physics of Fluids*, vol. 32, p. 076105, 2020.
15. E. Degregori and J. W. Kim, "Mitigation of transonic shock buffet on a supercritical airfoil through wavy leading edges," *Physics of Fluids*, vol. 33, p. 026104, 2021.
16. H. Liu, J.-H. Sun, C.-Y. Xu, X. Lu, Z. Sun, and D.-R. Zheng, "Numerical simulation and dynamic mode decomposition analysis of the flow past wings with spanwise waviness," *Engineering Applications of Computational Fluid Mechanics*, vol. 16, pp. 1849-1865, 2022.

17. S. S. Sidhu, A. Asghar, and W. D. Allan, "Performance Evaluation of Leading Edge Tubercles Applied to the Blades in a 2-D Compressor Cascade," in *Turbo Expo: Power for Land, Sea, and Air*, 2021, p. V02AT31A017.
18. F. R. Butt and T. Talha, "Numerical investigation of the effect of leading-edge tubercles on propeller performance," *Journal of Aircraft*, vol. 56, pp. 1014-1028, 2019.
19. C. Stark, W. Shi, and M. Atlar, "A numerical investigation into the influence of bio-inspired leading-edge tubercles on the hydrodynamic performance of a benchmark ducted propeller," *Ocean Engineering*, vol. 237, p. 109593, 2021.
20. L. Du, R. G. Dominy, and G. Ingram, "Experimental Investigation of the Performance of H-Darrieus Wind Turbines With Tubercle Leading Edge Blades," in *Turbo Expo: Power for Land, Sea, and Air*, 2020, p. V012T42A001.
21. A. N. Gonçalves, J. M. Pereira, and J. M. Sousa, "Passive control of dynamic stall in a H-Darrieus Vertical Axis Wind Turbine using blade leading-edge protuberances," *Applied Energy*, vol. 324, p. 119700, 2022.
22. J. Joseph and A. Sathyabhama, "Leading edge tubercle on wind turbine blade to mitigate problems of stall, hysteresis, and laminar separation bubble," *Energy Conversion and Management*, vol. 255, p. 115337, 2022.
23. W. Ke, I. Hashem, W. Zhang, and B. Zhu, "Influence of leading-edge tubercles on the aerodynamic performance of a horizontal-axis wind turbine: A numerical study," *Energy*, vol. 239, p. 122186, 2022.
24. I. C. M. Lositaño and L. A. M. Danao, "Steady wind performance of a 5 kW three-bladed H-rotor Darrieus Vertical Axis Wind Turbine (VAWT) with cambered tubercle leading edge (TLE) blades," *Energy*, vol. 175, pp. 278-291, 2019.
25. I. Ali, T. Hussain, I. N. Unar, and M. Waqas, "Aerodynamic performance analysis of the wavy wing with varying spanwise waviness characteristics," *Bulletin of the American Physical Society*, 2022.
26. S. Sridhar, J. Joseph, and J. Radhakrishnan, "Implementation of tubercles on Vertical Axis Wind Turbines (VAWTs): An Aerodynamic Perspective," *Sustainable Energy Technologies and Assessments*, vol. 52, p. 102109, 2022.
27. Z. Wang and M. Zhuang, "Leading-edge serrations for performance improvement on a vertical-axis wind turbine at low tip-speed-ratios," *Applied Energy*, vol. 208, pp. 1184-1197, 2017.
28. Y. Zhang, Z. Guo, X. Zhu, Y. Li, X. Song, C. Cai, *et al.*, "Investigation of aerodynamic forces and flow field of an H-type vertical axis wind turbine based on bionic airfoil," *Energy*, vol. 242, p. 122999, 2022.
29. Y. Zhang, X. Zhu, X. Song, C. Cai, T. Zhou, Y. Kamada, *et al.*, "Effect of the bionic blade on the flow field of a straight-bladed vertical axis wind turbine," *Energy*, vol. 258, p. 124834, 2022.
30. S. S. ul Hassan, M. T. Javaid, U. Rauf, S. Nasir, A. Shahzad, and S. Salamat, "Systematic investigation of power enhancement of Vertical Axis Wind Turbines using bio-inspired leading edge tubercles," *Energy*, vol. 270, p. 126978, 2023.
31. W. Shi, M. Atlar, and R. Norman, "Detailed flow measurement of the field around tidal turbines with and without biomimetic leading-edge tubercles," *Renewable Energy*, vol. 111, pp. 688-707, 2017.
32. W. Shi, M. Atlar, R. Norman, B. Aktas, and S. Turkmen, "Numerical optimization and experimental validation for a tidal turbine blade with leading-edge tubercles," *Renewable Energy*, vol. 96, pp. 42-55, 2016.

33. W. Shi, M. Atlar, R. Norman, S. Day, and B. Aktas, "Effect of waves on the leading-edge undulated tidal turbines," *Renewable energy*, vol. 131, pp. 435-447, 2019.
34. I. Tunio, D. Kumar, T. Hussain, and M. Jatoi, "Investigation of variable spanwise waviness wavelength effect on wing aerodynamic performance," *Fluid Dynamics*, vol. 55, pp. 657-669, 2020.
35. Z. Wei, J. Toh, I. Ibrahim, and Y. Zhang, "Aerodynamic characteristics and surface flow structures of moderate aspect-ratio leading-edge tubercled wings," *European Journal of Mechanics-B/Fluids*, vol. 75, pp. 143-152, 2019.
36. D. Serson, J. Meneghini, and S. Sherwin, "Direct numerical simulations of the flow around wings with spanwise waviness at a very low Reynolds number," *Computers & Fluids*, vol. 146, pp. 117-124, 2017.
37. A. Corsini, G. Delibra, and A. G. Sheard, "On the role of leading-edge bumps in the control of stall onset in axial fan blades," *Journal of fluids engineering*, vol. 135, p. 081104, 2013.
38. I. Fernandes, Y. Sapkota, T. Mammen, A. Rasheed, C. Rebello, and Y. H. Kim, "Theoretical and experimental investigation of leading edge tubercles on the wing performance," in *2013 Aviation Technology, Integration, and Operations Conference*, 2013, p. 4300.
39. A. F. A. Gawad, "Utilization of whale-inspired tubercles as a control technique to improve airfoil performance," *Transaction on control and mechanical systems*, vol. 2, pp. 212-218, 2013.
40. I. Tunio, D. Kumar, T. Hussain, M. Jatoi, and Safiullah, "Investigation of variable spanwise waviness wavelength effect on wing aerodynamic performance," *Fluid Dynamics*, vol. 55, pp. 657-669, 2020.
41. M. Fan, X. Dong, Z. Li, Z. Sun, and L. Feng, "Numerical and experimental study on flow separation control of airfoils with various leading-edge tubercles," *Ocean Engineering*, vol. 252, p. 111046, 2022.
42. Y.-y. Wang, W.-r. Hu, and S.-d. Zhang, "Performance of the bio-inspired leading edge protuberances on a static wing and a pitching wing," *Journal of hydrodynamics*, vol. 26, pp. 912-920, 2014.